HHS Public Access

Author manuscript

Ann Biomed Eng. Author manuscript; available in PMC 2024 March 01.

Published in final edited form as:

Ann Biomed Eng. 2023 March ; 51(3): 566–577. doi:10.1007/s10439-022-03064-2.

Cryopreservation of whole rat livers by vitrification and nanowarming

Anirudh Sharma[1,#], **Charles Y. Lee**[2,3,#], **Bat-Erdene Namsrai**[4], **Zonghu Han**[1], **Diane Tobolt**[4], **Joseph Sushil Rao**[4,5], **Zhe Gao**[1], **Michael Etheridge**[1], **Michael Garwood**[6], **Mark G. Clemens**[2,7], **John C. Bischof**[1,†], **Erik B. Finger**[4,†]

[1]Department of Mechanical Engineering, University of Minnesota; Minneapolis, MN, 55455, USA.

[2]Department of Mechanical Engineering and Engineering Science; University of North Carolina; Charlotte, NC, 28223, USA.

[3]Center for Biomedical Engineering and Science, University of North Carolina, Charlotte, NC 28223, USA

[4]Department of Surgery, University of Minnesota; Minneapolis, MN, 55455, USA.

[5]Schulze Diabetes Institute, University of Minnesota; Minneapolis, MN, 55455, USA.

[6]Center for Magnetic Resonance Research, Department of Radiology, University of Minnesota; Minneapolis, MN, 55455, USA.

[7]Department of Biological Sciences, University of North Carolina, Charlotte, NC 28223, USA

Abstract

Liver cryopreservation has the potential to enable indefinite organ banking. This study investigated vitrification—the ice-free cryopreservation of livers in a glass-like state—as a promising alternative to conventional cryopreservation, which uniformly fails due to damage from ice formation or cracking. Our unique “nanowarming” technology, which involves perfusing biospecimens with cryoprotective agents (CPAs) and silica-coated iron oxide nanoparticles (sIONPs) and then, after vitrification, exciting the nanoparticles via radiofrequency waves, enables rewarming of vitrified specimens fast enough to avoid ice formation and uniformly enough to prevent cracking from thermal stresses, thereby addressing the two main failures of conventional cryopreservation. This study demonstrates the ability to load rat livers with both CPA

Corresponding author: Erik B. Finger, MD, PhD, Division of Solid Organ Transplantation, University of Minnesota, 420 Delaware St. S.E., MMC 195, Minneapolis, MN 55455, Phone: (612) 626-1154, Fax: (612) 624-7168, efinger@umn.edu.
[#]These authors contributed equally to this work.
[†]These authors contributed equally to this work as co-senior authors

Ethics declarations

Conflict of interest: The authors (Sharma, Lee, Etheridge, Bischof, Finger) declare patents issued and pending related to the described methodology.

Supplementary Materials statement: Additional detail is presented in a Supplementary Materials section.

and sIONPs by vascular perfusion, cool them rapidly to an ice-free vitrified state, and rapidly and homogenously rewarm them. While there was some elevation of liver enzymes (Alanine Aminotransferase (ALT)) and impaired indocyanine green (ICG) excretion, the nanowarmed livers were viable, maintained normal tissue architecture, had preserved vascular endothelium, and demonstrated hepatocyte and organ-level function, including production of bile and hepatocyte uptake of ICG during normothermic reperfusion. These findings suggest that cryopreservation of whole livers via vitrification and nanowarming has the potential to achieve organ banking for transplant and other biomedical applications.

Keywords

Organ preservation; Liver transplant; Critical cooling rate; Critical warming rate; Cryoprotective agent

Introduction

Liver transplantation is the best treatment option in terms of life expectancy and quality of life for people with end-stage liver disease. Unfortunately, there remains a large and growing gap between organ supply and demand[41]; yet many thousands of livers go unused each year, particularly from expanded criteria donors (ECD) who are older, have experienced cardiac death (i.e., donation after circulatory death, DCD), or have other complications associated with inferior postoperative outcomes[27]. These organs would be valuable for therapeutic and research purposes, including transplantation, if not for their increased susceptibility to ischemic preservation injury and short tolerable preservation times, typically <12 hours for optimal donors and even less for ECD and DCD donors.

Organ cryopreservation could enable indefinite organ storage[16, 34] and mitigate the ischemic damage between organ recovery and use. These livers could then be available on-demand for transplantation or to produce cells and component parts for other therapeutic and diagnostic applications such as hepatocyte transplantation[18, 25], bioartificial liver devices[1, 35], emergency segmental auxiliary liver grafts[7], drug discovery and toxicity testing[29, 44], and basic hepatic pathophysiology research.

Conventional methods for cryopreservation of cells and tissues utilize slow cooling to a frozen state, resulting in the formation of ice crystals that damage cells and disrupt the complex macroscopic organization of intact organs[6, 37] making these methods ineffective for liver cryopreservation.

A promising alternative to conventional cryopreservation is *vitrification*, or rapid cooling to a “glassy” rather than crystalline phase. Vitrified materials behave like solid materials but do not undergo the damaging phase transition from liquid to crystalline ice.In this form, biomaterials can be stored indefinitely in a deep cryogenic state (< −140 °C)[16].

To vitrify biospecimens, including organs, they must be cooled to below a glass transition temperature (T_g, ~ −120 °C) at a rate that is too fast for ice crystallization to occur. This rate is termed the critical cooling rate (CCR). In contrast, the critical warming rate (CWR)

is the rate necessary to avoid crystallization during warming, and is typically at least an order of magnitude higher than the CCR [23]. The CCR and CWR for physiologic solutions (e.g., water) are unachievable in organs (>106 °C/sec)[4], but fortunately, CPA compounds can reduce CCRs and CWRs to practical levels (<1 to 100s °C/min)[13, 26].

Small biologic units such as cells and embryos are routinely cryopreserved by vitrification, and some success has been achieved in vitrifying larger biological systems such as porcine arteries, rat and rabbit kidneys, and rat hearts[9, 17, 19, 24, 33, 40]. However, a more significant challenge occurs upon rewarming these biomaterials, especially as size increases. Rewarming must be rapid to avoid ice formation and uniform to cracking from thermomechanical stress, which are two significant obstacles for this approach. For biomaterials with a characteristic dimension >1 cm, traditional convective or "boundary" rewarming methods (i.e., immersion in a liquid bath) fail at achieving both objectives.

We have developed "nanowarming" as an alternative method to rewarm tissues and organs rapidly and uniformly through radiofrequency (RF) magnetic heating of iron oxide nanoparticles (IONPs) that are distributed throughout the vasculature. IONPs are exposed to alternating magnetic fields in the RF frequency range and exhibit rapid heating from hysteresis losses. Volumetric heating is uniform, occurs throughout the organ, and is not constrained by organ size. This approach provides a substantial advantage in that it can be directly scaled to human-sized organs. Previous studies on nanowarming of large artery segments[33] and CPA systems up to 80 mL, including rat kidneys and rat hearts, have resulted in high post-rewarming cell viability[9, 19, 40], but limited organ function has been demonstrated. Fig. 1 illustrates the principle of nanowarming.

Here we investigate vitrification and nanowarming of whole rat livers to maintain organ-level viability and function. The rat liver studied is one of the largest organs to be vitrified and rewarmed thus far. This study presents the following achievements: 1) perfusion delivery of CPA throughout the hepatic parenchyma; 2) perfusion loading of sIONPs within the liver vasculature; 3) rapid cooling at rates greater than CCR to achieve an ice-free vitrified state; 4) rapid (greater than CWR) and uniform rewarming that avoids ice formation (devitrification) or cracking; 5) perfusion unloading of both CPA and sIONPs; and finally, 6) assessment of viability, morphology, and function post-nanowarming.

Materials and Methods:

Cryoprotective agent and iron oxide nanoparticles

Biocompatible silica-coated iron oxide nanoparticles (sIONPs) were synthesized as previously described[20]. The CPA selected was 40% ethylene glycol (v/v%) plus 0.6 M sucrose (EG+Suc) in Euro-Collins (EC) solution carrier[10] (Table S2) based on previous success in vitrification of hepatocyte spheroids[28, 32] and superiority over alternative agents tested (i.e., VS55[38]) which had increased toxicity in preliminary experiments.

Animals and surgery

Animal experiments were approved by the Institutional Animal Care and Use Committee (IACUC) at the University of Minnesota. Experiments were performed under Isoflurane

anesthesia with male Sprague Dawley rats (Charles Rivers, Wilmington, MA) weighing 250–300 g. Donor livers were cannulated via the portal vein (PV), suprahepatic vena cava (SHVC), and the infrahepatic vena cava (IHVC), flushed with cold University of Wisconsin (UW) solution, and stored at 4 °C prior to use (details in Supplementary Materials). Cold storage time prior to study was ≤ 30 minutes.

Hypothermic perfusion

The perfusion circuit is described in detail elsewhere[40] and includes multiple perfusion channels, flow dampening, bubble trap, heat exchanger, and pressure and temperature monitoring and control. Stepwise loading of increasing concentrations of CPA (15 min steps at 4 °C) was performed via the PV (details in Supplementary Materials). Subsequently, sIONPs in CPA were infused via syringe pump at 1 mL/min after the final CPA loading step. For subsequent washout of sIONPs and CPA, serial dilutions of hypertonic sucrose in EC were used in 10-minute perfusion steps (Supplementary Table S3).

Vitrification

A polyethylene bag (McMaster-Carr, Elmhurst, IL) was prefilled with 25–30 ml of 5 or 10 mg Fe/mL sIONP in CPA and held at 0–4 °C. Following perfusion loading, cryogenic fiber optic temperature probes (Qualitrol, Fairport, NY) were placed inside the IHVC, PV, SHVC, and outside the liver before transfer to the bag. Organs were cooled to −150°C (see Supplementary Materials for cooling protocol) in a controlled-rate freezer (CRF) (Kryo560, Planer, Middlesex, UK) and stored for 1 hr to several days in a −150 °C freezer (Panasonic Healthcare, Wood Dale, IL) prior to rewarming.

Nanowarming

Nanowarming was conducted using a 15-kW alternating magnetic field (AMF) coil at 94% power (preset to 63 kA/m and 185 kHz)[33]. The vitrified liver was quickly transferred from the cryogenic freezer (−150 °C) to the center of the solenoid coil, and the AMF was turned on. The AMF was powered off when the temperature exceeded the melting temperature (T_m) of the CPA. After rewarming, stepwise unloading of CPA+sIONP was performed (Supplementary Table S3).

Normothermic perfusion for functional evaluation

Ex vivo organ function was assessed by normothermic perfusion with oxygenated Krebs-Henseleit (KH) buffer (full details in Supplementary Materials). Biliary output and venous effluents were collected for blood gas, compositional analysis, and subsequent LDH/Alanine Aminotransferase (ALT) assays at 15-minute intervals. Indocyanine green (ICG, an anionic dye actively taken up by hepatocytes and secreted into the bile) was added to the KH buffer at 25 mg/L to assess hepatocyte function. At the end of the perfusion, wedge biopsies were obtained for histology. ALT was quantified using a colorimetric ALT assay kit (Sigma, St. Louis, MO). LDH was measured using the LDH-Glo assay (Promega, Madison, WI). Experimental groups included fresh control organs (flushed with UW solution and stored at 4 °C for <30 min prior to study), static cold stored (SCS, 18–20 hrs storage in UW solution at 4 °C), CPA-only (CPA loaded and unloaded), and nanowarmed organs.

Histology, confocal, freeze substitution, and μCT imaging

Liver biopsy specimens were fixed, paraffin-embedded, sectioned, stained, and imaged by light microscopy (Hematoxylin and Eosin (H&E) and Prussian blue), confocal imaging (CD31 expression), and freeze-substitution (ice damage) as described in the Supplementary Materials. Cryogenic μCT imaging of whole livers was used to detect ice formation (devitrification), cracks, and sIONP distribution in the liver as previously described[40]., and detailed in the Supplementary Materials.

Statistical analysis

Statistical analysis was performed in R version 4.0.4 (R Foundation for Statistical Computing, Vienna, Austria). Continuous variables were tested for normality using the Shapiro Wilk test. One-way ANOVA with pairwise Tukey post-hoc testing was performed for normally distributed variables. The Kruskal-Wallis test with pairwise Mann-Whitney (Wilcoxon) post-hoc test was used for non-normal variables. P values were adjusted for multiple comparisons, and a value of <0.05 was considered significant. Data are presented as mean ± standard deviation (SD) unless noted otherwise. Informative statistical comparisons are indicated in each figure, and complete statistical treatment is summarized in the Supplementary Materials.

Results:

Perfusion loading and unloading of CPA+sIONPs

Liver perfusion loading of CPA (EG+Suc) was carried out via the portal vein at a flow rate of 0.3 mL/min/g liver, with the effluent being collected throughout. The mean portal venous pressure increased with every perfusion step, likely due to increased viscosity, but remained within acceptable physiological limits (0–10 mm Hg) (Fig. 2A). At the final loading step, the relative EG concentrations in the perfusate and venous effluents indicated near complete equilibration of CPA (Fig. 2B). Following full CPA loading, a colloidal mixture of 10 mg Fe/mL sIONPs in CPA was perfusion loaded into the liver at a constant rate of 1 mL/min.

Figs. 2C–K shows gross visual appearance, Prussian blue-stained histologic sections, and μCT images of control, CPA+sIONP loaded, and unloaded livers. As the CPA+sIONP colloid is loaded into the vasculature, the liver gradually changes color from brown to solid black, indicating saturation of the blood vessels with the dark sIONP nanoparticles. Prussian blue staining of histological liver slices showed that the sIONPs (blue) reside in the extracellular vascular space and are not taken up by the hepatocytes or other nonparenchymal cells. Cellular uptake was not expected to occur, as the CPA and sIONPs are loaded and unloaded at 4 °C and phagocytic activities would be minimal at these temperatures. sIONP localization was confirmed by μCT, which demonstrated sIONP accumulation in the vasculature, which showed high HU contrast within larger vascular structures (>29 μm resolution). Furthermore, an overall increase in diffuse background HU throughout the liver was observed compared to controls, which suggested loading within smaller vascular branches, and was confirmed by Prussian blue staining. Following washout, μCT and Prussian blue stains showed complete removal of the sIONPs at the detection limit of these modalities.

Vitrification

After loading with CPA+sIONPs, the liver-containing bags were transferred to a CRF and cooled rapidly to cryogenic temperature (−150 °C) (Fig. 3A). The cooling rates in all regions within the liver were observed to be faster than the CCR, with a mean cooling rate of 8.8 °C/min (Fig. 3B). For reference, the CCR of EG+Suc, shown as the red dotted line in Figs. 3A and 3B, is <1 °C/min (determined by differential scanning calorimetry, data not shown). Additionally, during cooling while in the glass region (below T_g, −121°C), the measured temperature difference between the liver surface and interior was very low (<5°C), much lower than a threshold for cracking (>15°C) that was empirically determined from rewarming experiments (Fig. 4).

The vitrified livers appeared glassy on gross visualization, with no visible ice crystals or cracks (Fig. 3E, top). High-resolution μCT imaging was used to verify vitrification success and the absence of crystallization or cracking (Fig. 3D). We have previously demonstrated the ability to distinguish between crystalline vs. amorphous phases in biological tissues at cryogenic temperatures based on X-ray attenuation[14]. High radiodensity (HU >500), which corresponds to the vitrified state, was observed within the liver (Fig. 3D, top), confirming the absence of ice crystals or cracks, which are generally characterized by lower radiodensity (<400 HU) and abrupt transitions in radiodensity, respectively (Fig. 3D, bottom). Additional examples of vitrified, frozen, and cracked livers are shown in Fig. S1.

To characterize the vitrified state at the cellular level, cryogenically cooled samples were processed by freeze-substitution prior to embedding, sectioning, and staining with toluidine blue (basic dye staining acidic cellular compartments, Fig. 3F). The vitrified liver showed near-normal tissue architecture with distinct hepatic acinar structures. Higher magnification of the section showed no ice crystal formation and hepatocytes (yellow asterisks) with intact nuclei. In addition, sinusoidal endothelial cells appeared preserved. In contrast, the frozen livers had significant disruption of cellular and macro-architecture. Punctate areas of white (red asterisks) indicate that ice had formed during cooling, both within and adjacent to the cells. Profound physical damage to the cells and the sinusoid boundaries was observed, and cellular debris was scattered throughout the frozen liver.

Nanowarming

Liver rewarming was accomplished using our previously described “nanowarming” methodology that uses magnetic nanoparticles (sIONP) that are distributed throughout the organ vasculature and can be excited by RF induced magnetic fields thus effectively providing volumetric rewarming [33]. The sIONP are biocompatible, colloidally stable in CPA solution, and can be flushed from the organ to an Fe level that is non-toxic [20, 47]. Innovations over our work in previous organs include modifying protocols for physical differences in the liver including the vascular supply, characterization of a CPA cocktail specifically for liver perfusion, and altered cooling and warming procedures to reduce the possibility of cracking.

Nanowarming of CPA+sIONP loaded livers typically took 120–140 seconds with a magnetic field intensity of 63kA/m at 185 kHz as the temperature profile was measured in different

regions of the liver (Figs. 4A–C). The mean warming rate within the livers during nanowarming was ~61°C/min, well above the CWR for the CPA (red dotted line), which is ~45 °C/min. No crystallization was observed during rewarming.

Due to their more extended structure (larger, flatter, and asymmetric) compared to other organs, livers may be more susceptible to cracking from thermal gradients developed during nanowarming. The rat liver is the largest organ to be vitrified and rewarmed by nanowarming thus far. In our initial testing, RF rewarming from low temperature (−150 °C) at near full power (63 kA/m and 185 kHz) resulted in a high thermal gradient, especially during the beginning of rewarming when the livers are most susceptible to cracking (i.e., below T_g) (Figs. 4E and S2). Cracking was observed in some cases, and we noted that the average maximum temperature difference between the surface and interior of the liver (ΔT_{max}) over the range from storage temperature (−150 °C) to T_g (~ −120 °C) was 22.5°C in the organs that cracked and 9.2 °C in those that did not (Fig. 4F). We experimentally defined an operational stress-to-fracture threshold ΔT_{max} of 15 °C for our CPA-loaded livers based on these data.

By modulating the RF power during rewarming, the average ΔT_{max} achieved within the liver while in a glassy state was reduced to 9.7 °C (Figs. 3D, E, and S2). Under this protocol, no visible cracking occurred. Further examples of temperature profiles for successfully rewarmed organs and those where cracking occurred are shown in Fig. S2.

Washout and reperfusion of nanowarmed livers

Following nanowarming, CPA and sIONP washout was performed by stepwise decrease in tonicity using sucrose solutions (Fig. 2A and additional details in Supplementary Materials). Portal venous pressure decreased with every washout step. Measurement of the effluent EG concentration (Fig. 2B) showed that EG levels were reduced below the refractometry detection limit by the end of washout, suggesting complete CPA unloading.

Following successful washout of the livers, normothermic reperfusion (at 37 °C) was performed over 60 minutes for functional assessment. Gross liver appearance showed that ICG was uniformly taken up throughout the liver (Figs. 5A–C, green staining), indicating preserved hepatocyte function and homogeneous perfusion. However, unlike control livers, ICG was not concentrated in the bile, indicating some compromise of bile canaliculi structure or hepatocyte ICG excretory function. Overall, bile effluent volumes measured in nanowarmed livers were comparable to CPA-loaded and unloaded livers (Fig. 5J).

To test for changes in tissue architecture or vascular damage, we performed histologic examination (Figs. 5D–F) and immunofluorescent staining for CD31 expression (Figs. 5G–I). Nanowarmed livers show intact cellular and sinusoidal architecture, comparable to controls. Bile ducts are present and normal in appearance with epithelial layer continuity maintained. The endothelium is preserved, as indicated by the positive CD31 staining (red) in >90% of the liver sections assessed. Further, physiological pressures observed under constant flow rates (pressure <12 mm Hg) support preserved vascular function (not shown). In contrast, convectively rewarmed livers showed intracellular and extracellular white space around hepatocytes (Fig. 5E, yellow arrows), indicating ice formation and cytoplasmic

vacuolization. CD31 staining was reduced or absent (Fig. 5H), suggesting damage to the endothelium.

ALT and LDH measurements in IVC effluent were used to assess hepatocyte injury (Fig. 5K–L). The ALT levels of nanowarmed livers were slightly higher than static cold-stored livers or fresh control livers, but comparable to CPA-only treated livers. LDH levels in venous effluent of nanowarmed livers were slightly higher only at the 15-minute time point but subsequently remained no different than any of the control groups. Notably, increases in ALT and LDH levels were relatively minor in comparison to other reports of liver injury during preservation[45] and in contrast to treatment with alternative CPA (VS55) which resulted in >10-fold higher values (not shown). These findings suggest that hepatocyte injury following vitrification and nanowarming is minor and may be due to CPA toxicity rather than ice formation or other damage occurring from the nanowarming process itself.

Discussion

Vitrification as a potential strategy for long-term cryopreservation was first conceptualized for cells in the 1930s[30] and later for organs in the 1980s[16]. However, apart from a report of transplant of a single rabbit kidney[17], it has not proved to be reliably achievable. The main limitation has been the inability to rewarm organs from the vitrified state while maintaining viability and function. Rapid and uniform rewarming is needed to avoid ice crystallization and cracking, respectively – something that is not achievable by simple convective heating technology. Here we have demonstrated successful vitrification and rewarming of whole rat livers with preserved tissue architecture, intact vascular endothelium, and indicators of hepatocyte and organ-level function (hepatocyte ICG uptake and bile production). Critical achievements on the way to this endpoint were the following: 1) success in perfusion loading of CPA loading throughout the liver parenchyma and sIONP in the vasculature, 2) cooling at a rate greater than CCR to achieve an ice-free vitrified state, 3) rewarming at a rate greater than CWR to avoid ice formation and with acceptable thermal gradients to void cracking, and 4) ability to unload CPA and sIONPs from nanowarmed livers.

The selection of CPA solutions requires a careful balance of their glass-forming ability (i.e., low CCR and CWR) and toxicity. The CPA used in this study (40% EG+0.6M sucrose) was well tolerated by the livers, and the cooling (8.8 °C/min) and rewarming (61 °C/min) rates achieved exceeded the CCR (<1 °C/min) and CWR (~45 °C/min) for this CPA. As predicted, under those conditions, we achieved ice-free vitrification and subsequent rewarming while preserving overall organ viability and function.

The nanowarming of the vitrified livers while avoiding ice formation and cracking was a significant achievement of this study. Using 10 mg Fe/mL sIONPs perfused throughout the vasculature resulted in rewarming rates sufficient to avoid ice formation during rewarming. Further, cracking from thermal stress was avoided when the temperature difference between the surface and interior was less than 15 °C. This temperature difference limit will be a vital consideration during scale up to larger livers, as the increased size of these organs will require a careful balance of high cooling rates (to avoid ice) and low thermal gradients (to prevent cracking).

sIONP were effectively removed from the organs during CPA unloading. Although Prussian blue and μCT did not indicate any residual sIONP in the liver, a small residual may persist below the detection limits for these assays. Future studies would be needed to address the quantity or impact of residual sIONP. However, in prior studies in rodents (with similar μCT appearance of unloaded organs), the residual sIONP content was non-toxic in vivo and was below equivalent FDA-approved levels for iron infusion in humans[20, 47]. Importantly, it should be noted that whereas CPA is distributed throughout the entire liver, sIONP remain only in the vascular lumens.

Post-nanowarming, we observed a differential effect on hepatocyte uptake of ICG and biliary excretion. Hepatocyte uptake in nanowarmed organs was comparable to control groups, indicating hepatocyte-specific function. However, while the organs did produce bile, ICG was not concentrated in the effluent as it was for the other control groups. This finding would suggest that the secretory or biliary function may have been compromised. Other measures (ALT, LDH, and histology) indicated minor, if any, injury to the hepatocytes or vasculature.

The differential susceptibility of hepatocytes and bile ducts to vitrification/nanowarming injury could be due to the liver's dual blood supply. Unlike other organs (e.g., kidneys) with a single vascular supply, the liver is perfused by both the portal vein and the hepatic artery. As is typical for rodent liver perfusion and transplant experiments, we only perfused via the portal vein in this study. Since the biliary system is primarily perfused from arterial branches, it is likely that the bile ducts had reduced CPA and fewer sIONPs than other parts of the liver. Thus, the bile ducts would have a higher effective CCR and CWR and a potentially decreased rewarming rate due to fewer sIONP, all of which would make them susceptible to ice formation and damage. Further studies are needed to address this potential concern, and dual perfusion (artery and PV) or retrograde biliary perfusion may be required. While bile ducts in nanowarmed livers appeared preserved, there may be specific changes in cell function (potentially due to CPA toxicity or regional differences in CPA concentration leading to ice formation), such as an impaired function of the active transport systems of hepatocytes or cholangiocytes. Further study of the physiologic changes of biliary excretion and composition of biliary effluent is ongoing.

Few reports exist for comparison to our study. We have previously demonstrated vitrification and nanowarming of rat kidneys and hearts [19, 40] and another group has tested a similar approach for rat hearts[9] (but with little/no biological characterization). The present report studied the largest organ (rat liver) reported thus far and demonstrated improved organ-level function compared to prior studies in the heart and kidney. While we have selected EG+Suc to use as a CPA in this study, other groups have studied alternative CPAs using precision-cut liver slices[11, 15, 22] which may have better glass-forming ability (i.e., lower CCR and CWR). Such agents may be required for vitrifying larger-sized organs. In contrast to our approach, a report from Gavish et al.[21] attempted cryopreservation of CPA-loaded rat and pig livers by slow freezing. While they reported bile production, normal architecture, and the ability to transplant an organ, insufficient data were presented to validate these claims, and there has been no follow-up study.

It is also important to compare our approach for organ preservation to other existing and developing technologies. Traditional static cold storage in UW solution (or similar preservation solutions) typically allows for up to 12 hours of liver preservation prior to transplant. In contrast, new techniques for hypothermic and normothermic machine perfusion may increase preservation times to 24 hours or longer and increase organ utilization[8, 31, 36, 43]. Further, strategies for high subzero organ storage have allowed liver preservation to be increased to 4 days for rat livers [5] and nearly 2 days with suboptimal human livers [12]. The same group demonstrated partial freezing of rat livers with preservation up to 5 days [42]. While these approaches are promising, preservation was extended by hours to days whereas organ preservation by vitrification is presumably indefinite. For this study, we stored vitrified livers for 1 hr to several days, but we have shown that other vitrified biomaterials can be stored at −150 °C for at least 9 months and function normally after transplant[46].

Another group has had some success with liver preservation using directional freezing [21]. Using slow freezing with 10% EG as a cryoprotectant, they were able to cryopreserve several rat and livers and demonstrate some bile production during normothermic perfusion in rat livers and following non-survival auxiliary transplant of a single thawed pig liver. Thawed rat livers showed relatively preserved histologic appearance. They also showed that they could isolate hepatocytes from those livers with viability between 50 and 90%. While those initial results were promising, there have not been any additional reports by that group in the liver. They have shown functional success with cryopreserving ovaries by their method [3, 39] and were able to transplant cryopreserved rat hindlimbs [2], albeit without restoration of function.

There are several limitations to our study. First, it was performed in the rat model, which may not reflect the size and complexity of larger systems (i.e., pig or human). Second, organ function was tested in vitro but not yet in vivo, which will be the subject of future study. Improvement (or decline) in organ function could be seen after transplant or even normothermic machine perfusion with blood. Third, we have not yet tested viability and measures of dysfunction at the cellular level (DNA fragmentation, apoptosis, changes in respiration and energy state, and viability). Fourth, we have not yet examined the function and viability of other nonparenchymal cells (e.g., Kupffer cells and stellate cells). Following future refinements in this approach it will be prudent to include a more detailed investigation of cellular and organ level function including measures of cell stress, injury, and death; biliary function such as bile composition and pH; synthetic function including albumin and clotting factor production; phase I and phase II metabolism; and others.

In conclusion, this study demonstrated the successful vitrification and rewarming of a rat liver using nanowarming technology. The livers had intact hepatic architecture and showed organ-specific function. However, improved preservation of the biliary system will need to be addressed in future studies. Nanowarming has many advantages over other strategies for rewarming vitrified organs and tissues, having the unique balance of rapid and uniform heating required to avoid ice crystallization and cracking. Further, nanowarming has the potential to directly scale from rodent organs to human-size organs simply by modifying the RF coil and energy supply. Having achieved the physical conditions for successful

vitrification and rewarming with notable biological function in the largest organ yet, future studies will need to address the delivery of the CPA and sIONP to the biliary system. In addition, we anticipate that, by optimizing the formulation and delivery conditions, we can achieve viable and functional whole liver cryopreservation and banking. The implications of such a potential advance are notable – the on-demand supply of organs when and where they are needed.

Supplementary Material

Refer to Web version on PubMed Central for supplementary material.

Acknowledgments:

This work was funded by NIH (HL135046, DK117425, DK131209, and DK126551) and NSF EEC 1941543. JSR acknowledges the support of the Schulze Diabetes Institute. We acknowledge the assistance of Dr. Mark Sanders of the University of Minnesota Imaging Center for assistance in freeze-substitution experiments.

Data availability:

The raw data required to reproduce these findings are available to download from Mendeley DOI 10.17632/9nsz5chp79.1.

Abbreviations:

ALT	alanine aminotransferase
AMF	alternating magnetic field
CRF	controlled rate freezer
CPA	cryoprotective agent
CCR	critical cooling rate
CWR	critical warming rate
DCD	donation after cardiac death
ECD	extended criteria donors
EC	Euro-Collins
EM	electromagnetic
EG	ethylene glycol
HU	Hounsfield units
ICG	indocyanine green
LDH	lactate dehydrogenase
μCT	micro-computed tomography

RF	radiofrequency
sIONP	silica coated iron oxide nanoparticles
T_g	glass transition temperature
T_m	melting temperature
UW	University of Wisconsin

References

1. Allen JW, Hassanein T. and Bhatia SN. Advances in bioartificial liver devices. Hepatology 34: 447–455, 2001. [PubMed: 11526528]
2. Arav A, Friedman O, Natan Y, Gur E. and Shani N. Rat Hindlimb Cryopreservation and Transplantation: A Step Toward “Organ Banking”. Am J Transplant 17: 2820–2828, 2017. [PubMed: 28422434]
3. Arav A, Gavish Z, Elami A, Natan Y, Revel A, Silber S, Gosden RG and Patrizio P. Ovarian function 6 years after cryopreservation and transplantation of whole sheep ovaries. Reprod Biomed Online 20: 48–52, 2010. [PubMed: 20158987]
4. Bald WB On crystal size and cooling rate. J Microsc 143: 89–102, 1986. [PubMed: 3531522]
5. Berendsen TA, Bruinsma BG, Puts CF, Saeidi N, Usta OB, Uygun BE, Izamis ML, Toner M, Yarmush ML and Uygun K. Supercooling enables long-term transplantation survival following 4 days of liver preservation. Nat Med 20: 790–793, 2014. [PubMed: 24973919]
6. Bischof JC Quantitative measurement and prediction of biophysical response during freezing in tissues. Annu Rev Biomed Eng 2: 257–288, 2000. [PubMed: 11701513]
7. Broelsch CE, Emond JC, Whitington PF, Thistlethwaite JR, Baker AL and Lichtor JL. Application of reduced-size liver transplants as split grafts, auxiliary orthotopic grafts, and living related segmental transplants. Ann Surg 212: 368–375; discussion 375–367, 1990. [PubMed: 2396888]
8. Ceresa CDL, Nasralla D, Knight S. and Friend PJ. Cold storage or normothermic perfusion for liver transplantation: probable application and indications. Curr Opin Organ Transplant 22: 300–305, 2017. [PubMed: 28301388]
9. Chiu-Lam A, Staples E, Pepine CJ and Rinaldi C. Perfusion, cryopreservation, and nanowarming of whole hearts using colloidally stable magnetic cryopreservation agent solutions. Sci Adv 7: 2021.
10. Collins GM, Bravo-Shugarman M. and Terasaki PI. Kidney preservation for transportation. Initial perfusion and 30 hours’ ice storage. Lancet 2: 1219–1222, 1969. [PubMed: 4187813]
11. de Graaf IA, Draaisma AL, Schoeman O, Fahy GM, Groothuis GM and Koster HJ. Cryopreservation of rat precision-cut liver and kidney slices by rapid freezing and vitrification. Cryobiology 54: 1–12, 2007. [PubMed: 17166492]
12. de Vries RJ, Tessier SN, Banik PD, Nagpal S, Cronin SEJ, Ozer S, Hafiz EOA, van Gulik TM, Yarmush ML, Markmann JF, Toner M, Yeh H. and Uygun K. Supercooling extends preservation time of human livers. Nat Biotechnol 37: 1131–1136, 2019. [PubMed: 31501557]
13. Elliott GD, Wang S. and Fuller BJ. Cryoprotectants: A review of the actions and applications of cryoprotective solutes that modulate cell recovery from ultra-low temperatures. Cryobiology 76: 74–91, 2017. [PubMed: 28428046]
14. Etheridge ML, Xu Y, Rott L, Choi J, Glasmacher B. and Bischof JC. RF heating of magnetic nanoparticles improves the thawing of cryopreserved biomaterials. Technology (Singap World Sci) 02: 229–242, 2014.
15. Fahy GM, Guan N, de Graaf IA, Tan Y, Griffin L. and Groothuis GM. Cryopreservation of precision-cut tissue slices. Xenobiotica 43: 113–132, 2013. [PubMed: 23106534]
16. Fahy GM, MacFarlane DR, Angell CA and Meryman HT. Vitrification as an approach to cryopreservation. Cryobiology 21: 407–426, 1984. [PubMed: 6467964]
17. Fahy GM, Wowk B, Pagotan R, Chang A, Phan J, Thomson B. and Phan L. Physical and biological aspects of renal vitrification. Organogenesis 5: 167–175, 2009. [PubMed: 20046680]

18. Forbes SJ, Gupta S. and Dhawan A. Cell therapy for liver disease: From liver transplantation to cell factory. J Hepatol 62: S157–169, 2015. [PubMed: 25920085]
19. Gao Z, Namsrai B, Han Z, Joshi P, Rao JS, Ravikumar V, Sharma A, Ring HL, Idiyatullin D, Magnuson EC, Iaizzo PA, Tolkacheva EG, Garwood M, Rabin Y, Etheridge M, Finger EB and Bischof JC. Vitrification and Rewarming of Magnetic Nanoparticle-Loaded Rat Hearts. Adv Mater Technol 7: 2100873, 2022.
20. Gao Z, Ring HL, Sharma A, Namsrai B, Tran N, Finger EB, Garwood M, Haynes CL and Bischof JC. Preparation of Scalable Silica-Coated Iron Oxide Nanoparticles for Nanowarming. Adv Sci (Weinh) 7: 1901624, 2020.
21. Gavish Z, Ben-Haim M. and Arav A. Cryopreservation of whole murine and porcine livers. Rejuvenation Res 11: 765–772, 2008. [PubMed: 18729808]
22. Guan N, Blomsma SA, van Midwoud PM, Fahy GM, Groothuis GM and de Graaf IA. Effects of cryoprotectant addition and washout methods on the viability of precision-cut liver slices. Cryobiology 65: 179–187, 2012. [PubMed: 22722061]
23. Han Z. and Bischof JC. Critical cooling and warming rates as a function of CPA concentration. CryoLetters 41: 185–193, 2020. [PubMed: 33988646]
24. Han Z, Sharma A, Gao Z, Carlson TW, O'Sullivan MG, Finger EB and Bischof JC. Diffusion Limited Cryopreservation of Tissue with Radiofrequency Heated Metal Forms. Adv Healthc Mater 9: e2000796, 2020.
25. Iansante V, Chandrashekran A. and Dhawan A. Cell-based liver therapies: past, present and future. Philos Trans R Soc Lond B Biol Sci 373: 2018.
26. Karow AM Jr. Cryoprotectants--a new class of drugs. J Pharm Pharmacol 21: 209–223, 1969. [PubMed: 4390139]
27. Klassen DK, Edwards LB, Stewart DE, Glazier AK, Orlowski JP and Berg CL. The OPTN Deceased Donor Potential Study: Implications for Policy and Practice. Am J Transplant 16: 1707–1714, 2016. [PubMed: 26813036]
28. Kuleshova LL, Wang XW, Wu YN, Zhou Y. and Yu H. Vitrification of encapsulated hepatocytes with reduced cooling and warming rates. Cryo Letters 25: 241–254, 2004. [PubMed: 15375435]
29. Li AP In vitro human hepatocyte-based experimental systems for the evaluation of human drug metabolism, drug-drug interactions, and drug toxicity in drug development. Curr Top Med Chem 14: 1325–1338, 2014. [PubMed: 24805059]
30. Luyet BJ The vitrification of organic colloids and of protoplasm. Biodynamica 1: 1–14, 1937.
31. MacConmara M, Hanish SI, Hwang CS, De Gregorio L, Desai DM, Feizpour CA, Tanriover B, Markmann JF, Zeh H 3rd and Vagefi PA. Making Every Liver Count: Increased Transplant Yield of Donor Livers Through Normothermic Machine Perfusion. Ann Surg 272: 397–401, 2020. [PubMed: 32694447]
32. Magalhaes R, Wang XW, Gouk SS, Lee KH, Ten CM, Yu H. and Kuleshova LL. Vitrification successfully preserves hepatocyte spheroids. Cell Transplant 17: 813–828, 2008. [PubMed: 19044208]
33. Manuchehrabadi N, Gao Z, Zhang J, Ring HL, Shao Q, Liu F, McDermott M, Fok A, Rabin Y, Brockbank KG, Garwood M, Haynes CL and Bischof JC. Improved tissue cryopreservation using inductive heating of magnetic nanoparticles. Sci Transl Med 9: 2017.
34. Mazur P. Freezing of living cells: mechanisms and implications. The American journal of physiology 247: C125–142, 1984. [PubMed: 6383068]
35. McKenzie TJ, Lillegard JB and Nyberg SL. Artificial and bioartificial liver support.Seminars in liver disease 28: 210–217, 2008. [PubMed: 18452120]
36. Nasralla D, Coussios CC, Mergental H, Akhtar MZ, Butler AJ, Ceresa CDL, Chiocchia V, Dutton SJ, García-Valdecasas JC, Heaton N, Imber C, Jassem W, Jochmans I, Karani J, Knight SR, Kocabayoglu P, Malagò M, Mirza D, Morris PJ, Pallan A, Paul A, Pavel M, Perera M, Pirenne J, Ravikumar R, Russell L, Upponi S, Watson CJE, Weissenbacher A, Ploeg RJ and Friend PJ. A randomized trial of normothermic preservation in liver transplantation. Nature 557: 50–56, 2018. [PubMed: 29670285]
37. Pegg DE Principles of cryopreservation. Methods Mol Biol 368: 39–57, 2007. [PubMed: 18080461]

38. Plitz J, Rabin Y. and Walsh JR. The Effect of Thermal Expansion of Ingredients on the Cocktails VS55 and DP6. Cell Preservation Technology 2: 215–226, 2004.

39. Revel A, Elami A, Bor A, Yavin S, Natan Y. and Arav A. Whole sheep ovary cryopreservation and transplantation. Fertil Steril 82: 1714–1715, 2004. [PubMed: 15589891]

40. Sharma A, Rao JS, Han Z, Gangwar L, Namsrai B, Gao Z, Ring HL, Magnuson E, Etheridge M, Wowk B, Fahy GM, Garwood M, Finger EB and Bischof JC. Vitrification and Nanowarming of Kidneys. Adv Sci (Weinh) 8: e2101691, 2021.

41. SRTR. Scientific Registry of Transplant Recipients National Data Report. 2021.

42. Tessier SN, de Vries RJ, Pendexter CA, Cronin SEJ, Ozer S, Hafiz EOA, Raigani S, Oliveira-Costa JP, Wilks BT, Lopera Higuita M, van Gulik TM, Usta OB, Stott SL, Yeh H, Yarmush ML, Uygun K. and Toner M. Partial freezing of rat livers extends preservation time by 5-fold. Nature communications 13: 4008, 2022.

43. van Rijn R, Schurink IJ, de Vries Y, van den Berg AP, Cortes Cerisuelo M, Darwish Murad S, Erdmann JI, Gilbo N, de Haas RJ, Heaton N, van Hoek B, Huurman VAL, Jochmans I, van Leeuwen OB, de Meijer VE, Monbaliu D, Polak WG, Slangen JJG, Troisi RI, Vanlander A, de Jonge J. and Porte RJ. Hypothermic Machine Perfusion in Liver Transplantation - A Randomized Trial. N Engl J Med 384: 1391–1401, 2021. [PubMed: 33626248]

44. Vinken M. and Hengstler JG. Characterization of hepatocyte-based in vitro systems for reliable toxicity testing. Arch Toxicol 92: 2981–2986, 2018. [PubMed: 30141065]

45. Xu H, Lee CY, Clemens MG and Zhang JX. Pronlonged hypothermic machine perfusion preserves hepatocellular function but potentiates endothelial cell dysfunction in rat livers. Transplantation 77: 1676–1682, 2004. [PubMed: 15201666]

46. Zhan L, Rao JS, Sethia N, Slama MQ, Han Z, Tobolt D, Etheridge M, Peterson QP, Dutcher CS, Bischof JC and Finger EB. Pancreatic islet cryopreservation by vitrification achieves high viability, function, recovery and clinical scalability for transplantation. Nat Med 28: 798–808, 2022. [PubMed: 35288694]

47. Zhang J, Ring HL, Hurley KR, Shao Q, Carlson CS, Idiyatullin D, Manuchehrabadi N, Hoopes PJ, Haynes CL, Bischof JC and Garwood M. Quantification and biodistribution of iron oxide nanoparticles in the primary clearance organs of mice using T1 contrast for heating. Magn Reson Med 78: 702–712, 2017. [PubMed: 27667655]

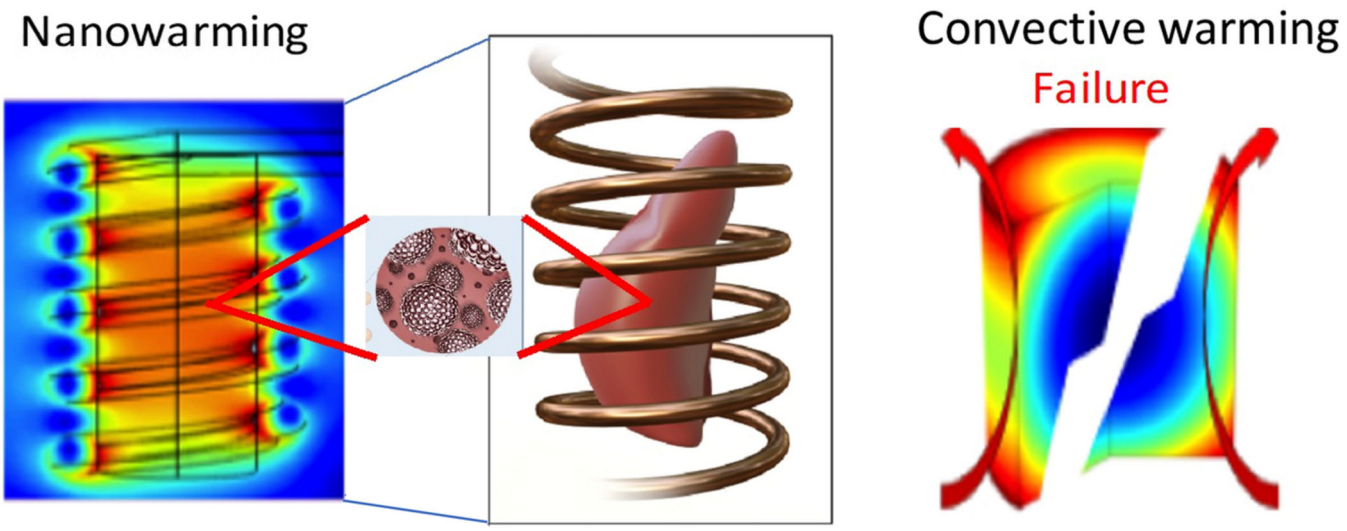

Figure 1. Conceptual schematic comparing nanowarming "volumetric" vs. convective "boundary" rewarming.

An alternating magnetic field in the RF frequency range (63 kA/m and 185 kHz) excites the magnetic nanoparticles within the CPA distributed in the organ vasculature. Heat is generated through hysteresis losses in the nanoparticles, which results in rapid and uniform rewarming. Notably, the fields in this frequency range do not cause significant direct heating of the biospecimen, so uniformity of heating is driven by the distribution of nanoparticles. Convective methods (right) typically fail to achieve rewarming rates faster than the CWR, causing damage from ice crystallization. Additionally, convective rewarming methods suffer from non- uniformity as the surface is rewarmed at much faster rates than the interior, leading to thermomechanical stresses and cracking.

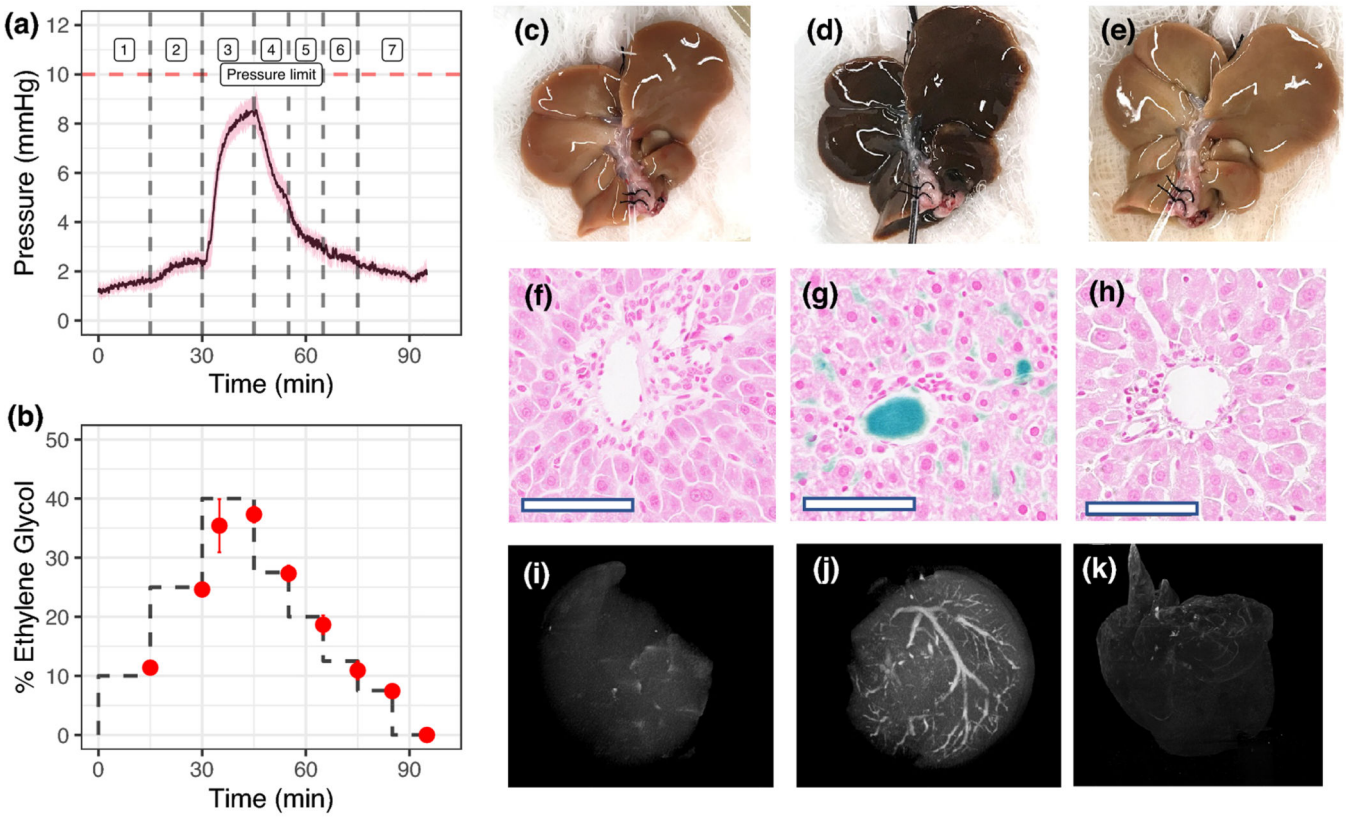

Figure 2. Hypothermic perfusion loading and unloading of cryoprotective agent (CPA) and silica coated iron oxide nanoparticles (sIONPs) in rat livers.

(A) Mean portal venous pressure over time during CPA (EG+Suc) loading and unloading in rat livers (steps in Table S3) (n = 6). **(B)** Percentage ethylene glycol in effluent samples collected from the IHVC during loading and unloading of CPA, determined by refractometry (n=4). **(C-E)** Gross images of control, CPA+sIONP loaded, and unloaded livers, respectively. **(F-H)** Prussian blue staining shows Fe deposition in control, CPA+sIONP loaded, and unloaded livers. Fe localization is seen in the liver sinusoids and the portal veins of a CPA+sIONP loaded liver. Bar = 100 μm. (**I-K**) X-ray μCT images of control, CPA+sIONP loaded, and unloaded livers, showing contrast from the iron oxide nanoparticles distributed throughout the liver vasculature (See Supplementary Materials files for 3D rotational images). Data are mean ± SEM.

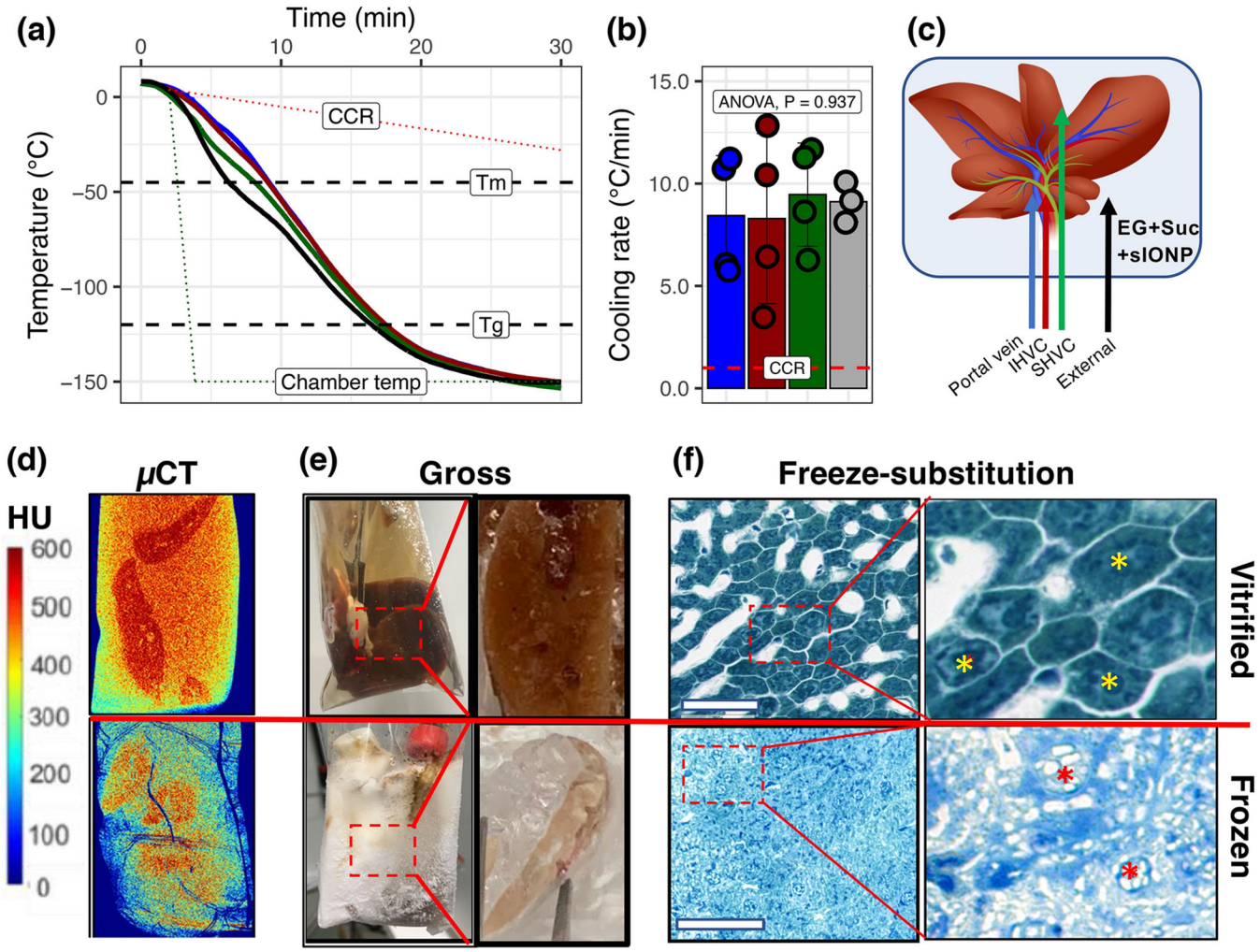

Figure 3. Vitrification of livers.

(A) Temperature vs. time plots during rapid cooling of a CPA-loaded liver for vitrification. Dashed lines indicate the critical cooling rate (CCR), melting temperature (T_m), glass transition temperature (T_g), and the temperature of the CRF (dotted line). **(B)** The average cooling rate for each probe location during cooling exceeds the CCR for CPA (EG+Suc) (dotted line). Data are mean ± SD (n = 4). **(C)** Position of the temperature probes for A and B within the liver. **(D)** X-ray μCT of a vitrified (top) vs. frozen (bottom) liver. X-ray attenuation, measured in Hounsfield Units (HU), was used to differentiate between amorphous (>400 HU) and crystalline regions (<400 HU) in the liver. For size reference, the cryobags are 3” x 5”. **(E)** Gross images of vitrified (top) and frozen (bottom) livers. Zoomed callout regions show gross tissue cross-sections of liver lobe pieces broken and exposed at cryogenic temperatures where a clear contrast was seen between vitrified vs. frozen. **(F)** Brightfield microscopy images of toluidine blue stained freeze-substituted liver sections following vitrification (top) and freezing (bottom) show intact cellular and sinusoidal architecture in vitrified samples and complete loss of architecture in both hepatocytes and sinusoidal endothelial cells in frozen livers. White space in the vitrified sample indicates the vasculature, whereas cells (yellow asterisks) show no ice. White space in the frozen samples

between and within cells (red asterisks) indicates the presence of vascular and intracellular ice. Bar = 100 μm.

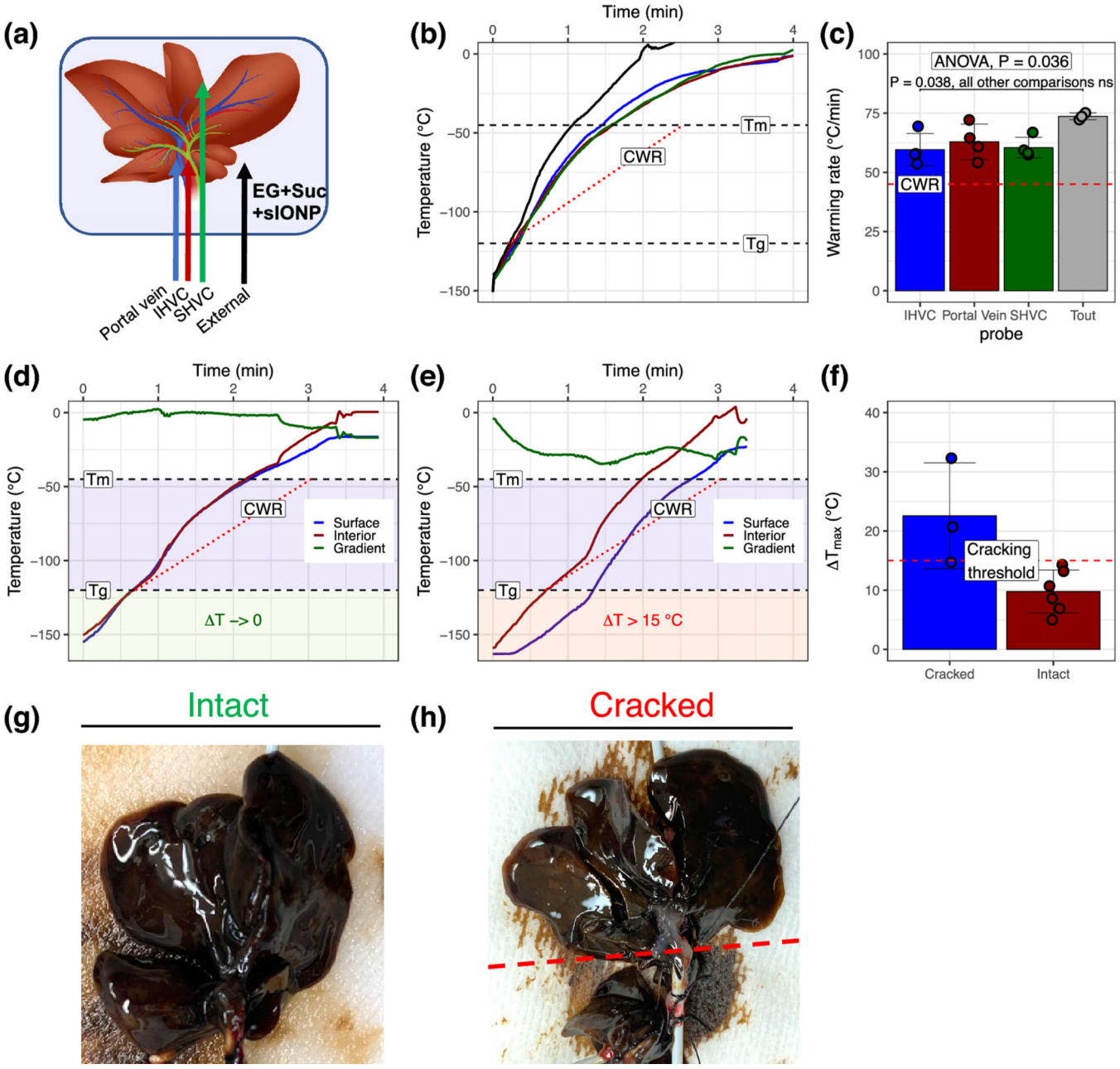

Figure 4. Rewarming of CPA and sIONP-loaded vitrified livers.

(A) Positioning of fluoroptic temperature probes within and around the liver. **(B)** Temperature vs. time recordings during nanowarming of vitrified rat livers show rewarming at rates exceeding the CWR of CPA (EG+suc) in all liver regions **(C)**. **(E)** During initial testing, rewarming was initiated from −150 °C at high power (63 kA/m, 185 kHz, right panel). A significant temperature difference (gradient) between the IHVC and the solution around the liver developed rapidly. This difference persisted through the glassy temperature zone (i.e., $<T_g$, red box), where the system is subject to thermal stress-induced cracking. Under these conditions, visible and audible cracking occurred in the livers **(H)**. **(D)** When the RF coil energy was initiated at low power between −150 °C and −115 °C (above

T_g, green box), temperature differences were much lower and cracking did not occur **(G)**. **(F)** The measured temperature differences from several experiments were compiled and correlated with the presence or absence of liver cracking. A cutoff of 15 °C was defined as the threshold for cracking. Data are mean ± SD (n = 3–6 per group).

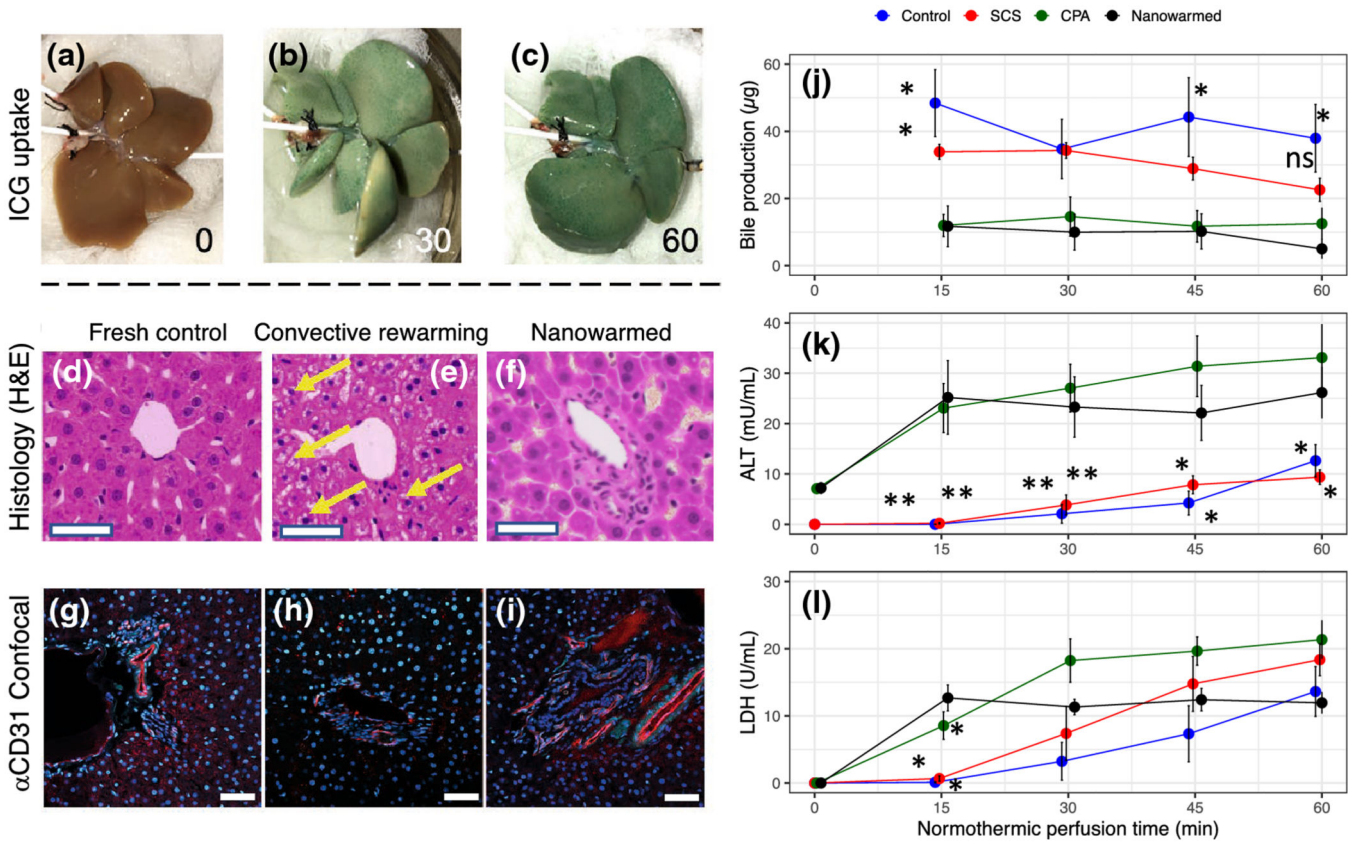

Figure 5. Organ-level function in vitrified and nanowarmed livers.

Vitrified and nanowarmed livers were tested for function and injury as compared to static cold storage (SCS, 18–20 hr in UW solution at 4 °C), CPA loaded and unloaded but not vitrified and untreated (flushed with UW and used within 30 min) controls. **(A-C)** Following washout of CPA+sIONP, the organs were assessed by normothermic machine perfusion with indocyanine green (ICG) in the perfusate and imaged at 0, 30, and 60 minutes. The nanowarmed livers demonstrated organ-level function with homogenous ICG uptake. **(D-F)** Histologic examination (hematoxylin and eosin) of control (left), vitrified and convectively rewarmed (middle), and vitrified and nanowarmed (right) livers show preserved tissue architecture in nanowarmed livers. Convectively rewarmed livers had diffuse areas of extra- and intracellular white space (yellow arrows) suggestive of ice crystallization during rewarming or cytoplasmic vacuolization. Nanowarmed livers have a normal portal and sinusoidal architecture. Bar = 100 μm. **(G-I**) Confocal imaging with anti-CD31 immunofluorescence shows that control and nanowarmed livers have preserved vascular architecture (red staining), whereas convectively rewarmed livers have reduced staining intensity, indicating endothelial injury. **(J)** Bile production assessed during 60 minutes of normothermic perfusion after nanowarming was not different than CPA-loaded and unloaded livers. Hepatocyte injury was assessed by measuring ALT **(K)** and LDH **(L)** in the SHVC venous effluent during perfusion. ALT levels for nanowarmed livers were slightly higher than for control organs throughout the normothermic perfusion, whereas LDH levels were not different between nanowarmed livers and other groups after 15 minutes. For all groups, n = 3–5. P values show comparison to nanowarming only with * = P <0.05 and ** = P

<0.01. All significant differences are shown. Full pairwise comparison statistics are in the Supplementary Materials.